

Sintering effect on varistor properties and degradation behavior of ZVMB varistor ceramics

Choon-W. Nahm¹

Received: 16 May 2017 / Accepted: 1 August 2017 / Published online: 7 August 2017
© Springer Science+Business Media, LLC 2017

Abstract ZnO–V₂O₅–Mn₃O₄–Bi₂O₃ (ZVMB) varistor ceramics were sintered at a low temperature range of 800–875 °C, and the microstructure, electrical properties, dielectric characteristics, and DC-accelerated aging behavior were systematically investigated. Analysis of the microstructure indicated that the average grain size increased from 3.8 to 6.4 μm with the increase of sintering temperature, and the density of the sintered pellets increased from 5.48 to 5.53 g/cm³ when the sintering temperature was increased from 800 to 850 °C, and then decreased when the sintering temperature was further increased. The breakdown field noticeably decreased from 13,412 to 706 V/cm with the increase of sintering temperature. The nonlinear coefficient exhibited a maximum value (43.0) at 825 °C and a minimum value (19.8) at 875 °C. The varistors sintered at 850 °C exhibited the highest stability; variation rates for the breakdown field and the nonlinear coefficient were –10.3 and –50.2%, respectively, after application of a stress of 0.85 E_{1mA}/85 °C/24 h.

1 Introduction

Varistor is voltage-dependent resistor, in which a resistance varies with applied voltage [1]. Just because a resistance varies with voltage does not mean it is a varistor, like general silicon diodes. It is called to varistor when a resistance abruptly changes with increasing voltage. Varistors involve

back-to-back Zener diode and the ceramics using grain boundary effect or interface effect. Zener diode is close to almost ideal varistor because of abrupt nonlinearity. However, Zener diode having a single junction is vulnerable to over-voltages such as surges. In real, semiconductor devices would be very susceptible or vulnerable to attack from various overvoltages. In contrast, ceramic varistors are mainly used to the surge protection due to high energy handling capability, when compared with back-to-back Zener diode [2–4]. Among them, zinc oxide varistors are typical ceramic varistors, which had been used for the longest time [1]. Zinc oxide varistors are featured by multi-junctions composed of grains and grain boundaries, which are distributed three dimensionally through sintered ceramics [2]. For this reason, zinc oxide varistors are extensively utilized to protect the electrical and electronic circuit system from abnormal overvoltage [5]. Today, all electrical and electronic systems have varistor's help.

Commercial zinc oxide varistors are mainly based on bismuth [1] and partially based on praseodymium inducing the varistor effect [6–9]. Zinc oxide ceramics incorporated with bismuth and praseodymium should be sintered at a high temperature above 1200 °C in order to exhibit the real function as varistors [1, 10]. In particular, multilayer varistors have no choice but to use a refractory such as Pd and Pt as an inner-electrode between multilayers. But, if the varistor ceramics can be sintered at a temperature as low as 900 °C, it is not necessary to use expensive Pd and Pt. Just, new zinc oxide ceramics incorporated with vanadium oxide (m.p 690 °C) inducing the varistor effect have a surprising advantage in terms of inner-electrode Ag [11, 12]. So-called, ZnO–V₂O₅-based ceramics can be sintered at a relatively low temperature in the vicinity of about 900 °C [11, 12]. This is very important for multilayer chip varistor applications because it

✉ Choon-W. Nahm
cwnahm@deu.ac.kr

¹ Semiconductor Ceramics Laboratory, Department of Electrical Engineering, Dongeui University, Busan 614-714, South Korea

can be co-sintered with an Ag inner-electrode without using expensive Pd or Pt.

ZnO–V₂O₅–MnO₂-based ceramics have been actively studied until now in order to improve nonlinear properties and stability [13–17]. However, ZnO–V₂O₅–Mn₃O₄-based ceramics were rarely studied [18–22]. Therefore, it is interesting to investigate how the sintering process has an effect on varistor properties for specific composition. There are no published reports studying the effect of the sintering temperature on the varistor properties in ZnO–V₂O₅–Mn₃O₄–Bi₂O₃ (ZVMB) varistor ceramics [23].

The aim of this paper is to investigate the effect of sintering temperature on the microstructure, electrical properties, dielectric characteristics, and DC-accelerated aging behavior of ZVMB varistor ceramics. In special, it shows that these varistor ceramics can be sintered at a low temperature as low as 800 °C.

2 Experimental procedure

2.1 Sample preparation

High-purity reagent-grade raw materials (>99.9%) in the proportion of 98.975 mol% ZnO+0.5 mol% V₂O₅+0.5 mol% Mn₃O₄+0.025 mol% Bi₂O₃ were prepared. The powders were mixed by ball milling with zirconia balls and acetone in a polypropylene bottle for 24 h. The mixed slurry was dried at 120 °C for 12 h, and the dried mixture was then mixed with acetone and polyvinyl butyral binder (0.8 wt% based on powder weight) in a beaker using a magnetic stirring bar. After drying at 120 °C for 24 h, the starting powder was produced by granulating the mixture by sieving through a 100-mesh screen. The powder was pressed into disc-shaped pellet of 10 mm in diameter and 1.5 mm in thickness at a pressure of 100 MPa. The pellets were set on MgO plate into alumina sagger, were sintered at four fixed sintering temperatures (800, 825, 850 and 875 °C) in air for 3 h, and were then furnace-cooled to room temperature. The sintered pellets were lapped and polished to 1.0 mm thickness using a lapping machine. The size of the final pellets was of 8 mm in diameter and 1.0 mm in thickness. Conductive silver paste was coated on both faces of the pellets by using screen-printing techniques, and electrodes of 5 mm in diameter were formed by heating at 550 °C for 10 min. Finally, after the lead wire was soldered on both electrodes, the samples were packaged by dipping it into a thermoplastic resin powder.

2.2 Microstructure analysis

Both sides of the samples were lapped and ground with SiC paper, and then polished with 0.3 μm–Al₂O₃ powders. The polished samples were chemically etched at HClO₄–H₂O

solution (1:1000, v/v) for 25 s at 25 °C. The microstructure of the surface was examined by a field emission scanning electron microscope (FESEM, Quanta 200, FEI, Brno, Czech). The average grain size (*d*) was determined by the lineal intercept method through the expression, $d = 1.56 LMN$, where *L* is the random line length on the micrograph, *M* is the magnification of the micrograph, and *N* is the number of the grain boundaries intercepted by the lines [24]. The crystalline phases were identified by X-ray diffractometer (XRD, X'pert-PRO MPD, Panalytical, Almelo, the Netherlands) with Cu K_α radiation. The density (*ρ*) of sintered pellets was measured using a density determination kit (238490) attached to balance (AG 245, Mettler Toledo International Inc., Greifensee, Switzerland).

2.3 Electrical measurement

The electric field–current density (*E*–*J*) characteristics were measured using a high voltage source unit (Keithley 237, Keithley Instruments Inc., Cleveland, OH, USA). The breakdown field (*E*_{1mA}) was measured at 1.0 mA/cm² and the leakage current density (*J*₁) was measured at 0.8 *E*_{1mA}. The nonlinear coefficient (*α*) was determined in the current density range 1.0–10 mA/cm², where $\alpha = (\log J_2 - \log J_1) / (\log E_2 - \log E_1)$, and *E*₁ and *E*₂ are the electric fields corresponding to 1.0 and 10 mA/cm², respectively.

2.4 Dielectric characteristic measurement

The dielectric characteristics, such as the apparent dielectric constant (*ε*_{APP}) and dissipation factor (tanδ) were measured in the range of 50 Hz–2 MHz using an RLC meter (Quad-Tech 7600).

2.5 DC-accelerated aging characteristic measurement

The DC-accelerated aging stress test for the samples was performed under the stress state of 0.85 *E*_{1mA}/85 °C/24 h. Simultaneously, the leakage current was monitored at intervals of 1 min during the stress test using a high voltage source-measure unit (Keithley 237, Cleveland, OH, USA). After application of a stress, the *E*–*J* characteristics were measured at room temperature.

3 Results and discussion

Figure 1 shows the cross-sectional SEM micrographs of the samples sintered at various temperatures from 800 to 875 °C. The average grain size increased from 3.8 to 6.4 μm despite the narrow range of sintering temperature with the increase of sintering temperature. The XRD patterns of the samples sintered at various temperatures are shown in Fig. 2. Analysis

Fig. 1 SEM micrographs of the samples sintered at various temperatures

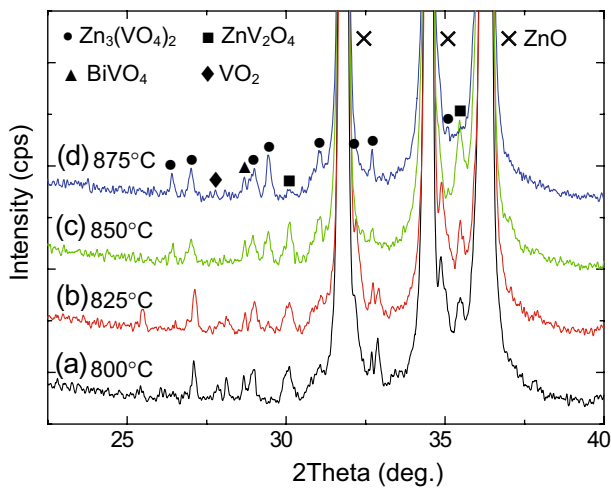
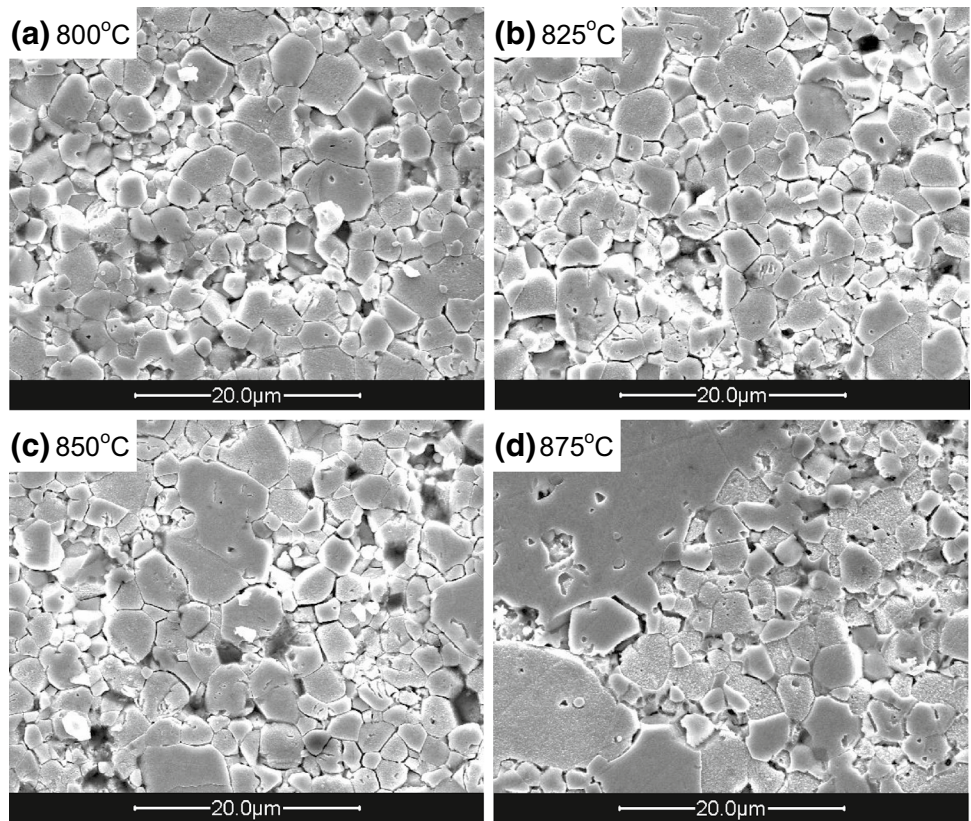
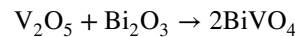
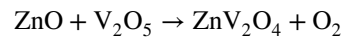
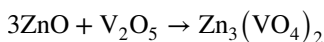


Fig. 2 XRD patterns of the samples sintered at various temperatures

of XRD peaks indicated that all samples involve $Zn_3(VO_4)_2$, ZnV_2O_4 , VO_2 , and $BiVO_4$ as the secondary minor phases. It can be seen that all minor phases were related to V-species. They are formed by liquid-phase sintering agent (V_2O_5) and act as a liquid-phase sintering aid. The secondary phases were formed by the following chemical reaction.



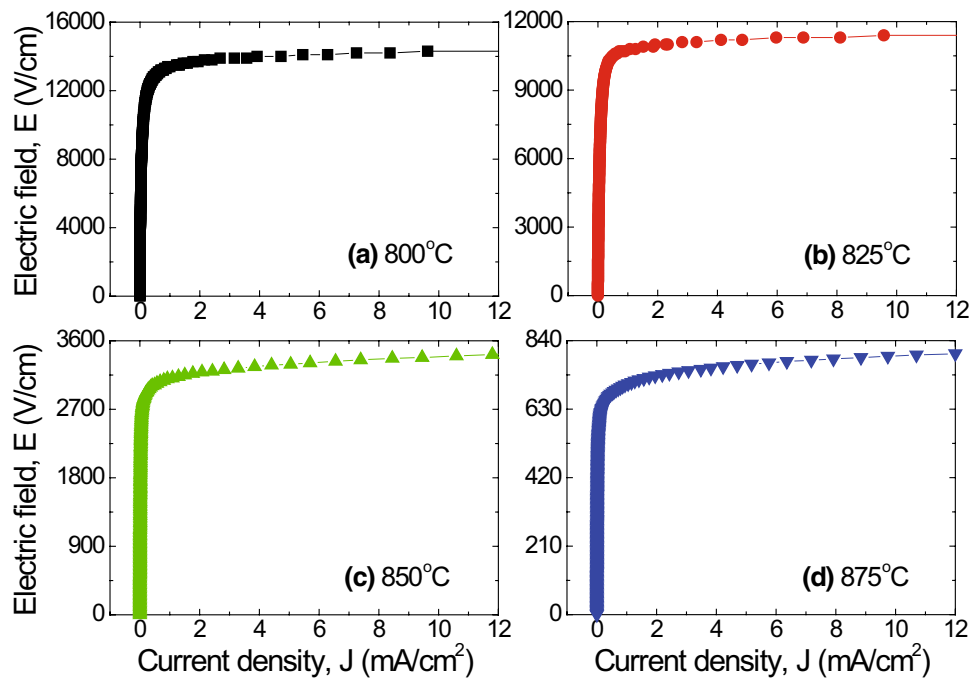
Among minor phases, ZnV_2O_4 and VO_2 were found to be the most greatly affected by sintering temperature. The peaks of ZnV_2O_4 ($2\theta = 30.0933^\circ$ and 35.4420°) and VO_2 ($2\theta = 28.0879^\circ$) decreased with the increase of sintering temperature. They were almost disappeared when the sintering temperature exceeded $875^\circ C$. On the other hand, the density of the sintered pellets increased from 5.48 to 5.53 g/cm^3 (theoretical density 5.78 g/cm^3 for ZnO) when the sintering temperature was increased from 800 to $850^\circ C$, and then decreased when the sintering temperature was further increased. The decrease of sintered density is assumed to be a result of the volatility of V-species for V_2O_5 with low melting point ($690^\circ C$). The detailed microstructural parameters are summarized in Table 1.

Figure 3 shows the E–J characteristics of the samples sintered at various temperatures. The E–J characteristics are the most important varistor properties, which are inherently characterized by non-linearity. The E–J curves are saliently divided into a non-conduction region and a conduction region. This division is assumed to be result of the presence of double Schottky barrier at grain boundaries.

Table 1 Average grain size (d), sintered density (ρ), breakdown field (E_{1mA}), breakdown voltage per grain boundaries (v_{gb}), nonlinear coefficient (α), leakage current density (J_L), apparent dielectric constant ($\epsilon_{APP'}$), and dielectric dissipation factor ($\tan\delta$) of the samples sintered at various temperatures

Sintering temp. (°C)	d (μm)	ρ (g/cm^3)	E_{1mA} (V/cm)	v_{gb} (V/gb)	α	J_L (mA/cm^2)	$\epsilon_{APP'}$ (1 kHz)	$\tan\delta$ (1 kHz)
800	3.8	5.48	13,412	5.1	38.0	0.13	405.6	0.249
825	4.2	5.51	10,797	4.5	43.0	0.15	543.3	0.248
850	4.9	5.53	3104	1.5	25.9	0.04	890.2	0.241
875	6.4	5.45	706	0.46	19.8	0.06	3018.8	0.223

Fig. 3 E–J characteristics of the samples sintered at various temperatures



A non-conduction region is explained by thermionic emission mechanism dominated by temperature dependence over a Schottky barrier, and a conduction region is explained by quantum mechanical tunneling mechanism dominated by field-dependence through a Schottky barrier.

The breakdown field (E_{1mA}) noticeably decreased from 13,412 to 706 V/cm with the increase of sintering temperature. The samples sintered at the temperature range of 800–825 °C exhibited high E_{1mA} exceeding 10 kV/cm. By the way, the sample sintered at a temperature as high as 25 °C than 825 °C decreased to E_{1mA} as low as about 300 V/cm. In light of this result, ZVMB ceramics show that the sintering temperature has a strong effect on the breakdown field (E_{1mA}) in spite of small variation of sintering temperature, when compared with other varistor ceramics. The decrease of E_{1mA} with the increase of sintering temperature is assumed to be a result of the decrease in the number of grain boundaries due to the increase in the average ZnO grain size (d) and the decrease of the

breakdown voltage per grain boundary (v_{gb}). This can be indicated in the expression,

$$E_{1mA} = v_{gb}/d.$$

The nonlinear coefficient (α) means a performance figure of varistor effect-itself. It is estimated at the vicinity of knee in the E–J characteristic curves. With the sintering temperature increased, the nonlinear coefficient increased from 38 to 43 until the sintering temperature is 825 °C. When the sintering temperature exceeded 825 °C, the breakdown field decreased to 19.8 at 875 °C. α of the samples sintered at 800–825 °C is remarkable value, when considered not only quaternary ceramics, but also low sintering temperature. ZVMB ceramics exhibit a higher α value than ZnO–V₂O₅–Mn₃O₄–Dy₂O₃ (or La₂O₃) ceramics exhibiting the best nonlinear properties ($\alpha = 33$) reported until now [18]. The behavior of α with sintering temperature can be related to the variation of the Schottky barrier height according to the variation of the electronic states at the grain boundaries. The sintering

temperature will vary the density of the interface states with the transport of the defect ions such as V and Mn species toward the grain boundary and will make more active grain boundaries. Therefore, the increase/decrease of α with the increase of sintering temperature is assumed to be a result of the increase/decrease of the barrier height at grain boundaries. On the other hand, the samples sintered in the range of 800–825 °C exhibited much higher leakage current density (J_L) than 0.1 mA/cm². However, the samples sintered at 850–875 °C exhibited about 50 μ A/cm². This behavior of J_L value becomes contrary to expectations in the light of α value. In light of this fact, the sintering temperature in the range of 800–825 °C is likely to increase the recombination current at the space charge layer. The detailed E–J characteristic parameters are summarized in Table 1.

Figure 4 shows the apparent dielectric constant (ϵ_{APP}) and dissipation factor ($\tan\delta$) of the samples sintered at various temperatures. ϵ_{APP} for all samples decreased in different variation rates with increasing frequency. The decrease of ϵ_{APP} with increasing frequency is assumed to be a result

of the decrease of the number of dipole, which can follow to specified frequency. The variation rates of ϵ_{APP} with increasing frequency increased when the sintering temperature increased. This is assumed to be a result of the increase of the viscosity resistance of ceramics with the increase of sintering temperature.

On the other hand, the increase of sintering temperature increased ϵ_{APP} in the range of test frequency. This is strongly dependent on the average grain size and depletion layer width, as can be seen in the expression, $\epsilon_{APP} = \epsilon_g(d/t)$, where ϵ_g is the dielectric constant of ZnO (8.5), d is the average grain size, and t is the depletion layer width of both sides at the grain boundaries. The ϵ_{APP} will be increased or decreased because the d/t ratio increases or decreases with the increase in sintering temperature. ϵ_{APP} at 1 kHz increased from 405.6 to 3018.8 at with the increase of sintering temperature.

With increasing frequency, $\tan\delta$ decreased until the vicinity of 13 kHz, again increased until the vicinity of 300–500 kHz, and then decreased when the frequency was further increased. In general, $\tan\delta$ exhibits a fluctuation with frequency. The abnormal dispersion of ϵ_{APP} appears at the peak of $\tan\delta$ and then the frequency is the vicinity of 300–500 kHz. $\tan\delta$ at 1 kHz increased from 0.249 to 0.223 with the increase of sintering temperature. However, on the whole, the sintering temperature led to the fluctuation for $\tan\delta$. The detailed dielectric characteristic parameters are summarized in Table 1.

Figure 5 shows the leakage current (I_L) behavior of the samples during application of the DC-accelerated aging stress of 0.85 $E_{1mA}/85$ °C/24 h. The I_L for all samples gradually increases with the increase of the stress time, and this shows that the varistors are gradually being degraded. The increase of I_L with increasing stress time is assumed

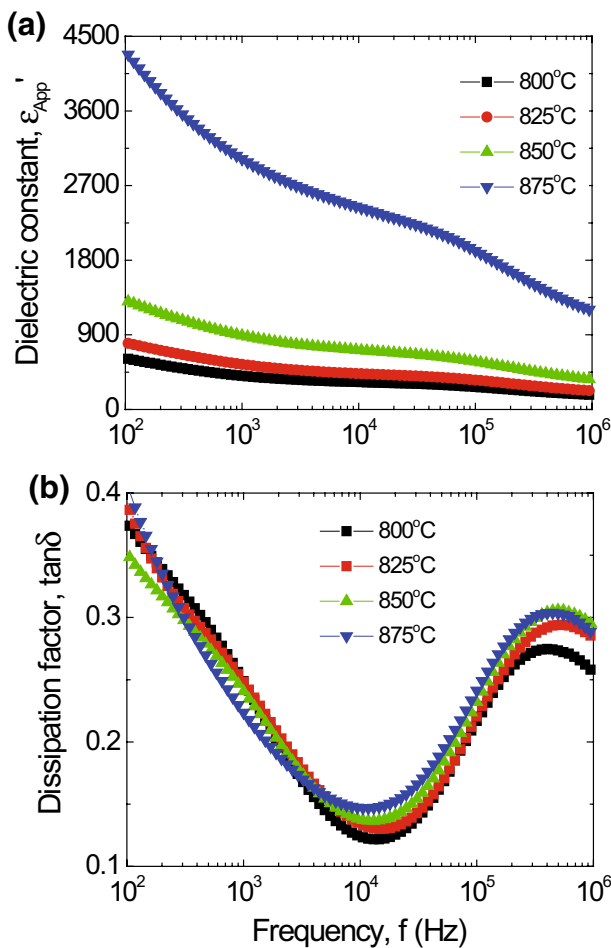


Fig. 4 Dielectric characteristics of the samples sintered at various temperatures

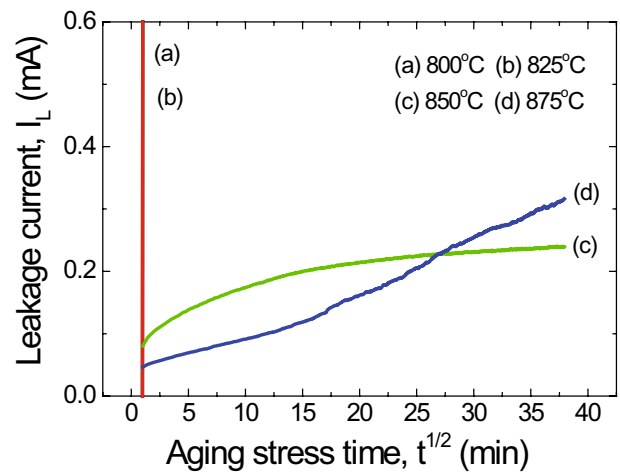


Fig. 5 Leakage current behavior during DC-accelerated aging stress of the samples sintered at various temperatures

to be a result of the increase of thermionic emission over a Schottky barrier due to the increase of ambient temperature. The samples sintered at 800 and 825 °C were destroyed due to the thermal runaway in an extremely short time as soon as application of a stress. In general, the stability is strongly affected by two factors, such as the sintered density and the leakage current. The higher sintered density and the lower leakage current will lead to the higher stability. The low sintered density decreases the number of parallel conduction paths and eventually leads to the concentration of current. The high leakage current easily increases joule heat, and joule heat also increases leakage current. Therefore, repetition cycle between joule heating and leakage current will lead to a thermal runaway. This is core for aging mechanism from a macroscopic viewpoint. Considering this content, it can be seen the reason why the samples sintered at 800 and 825 °C causes the thermal runaway. The I_L of the samples sintered at 850 °C is saturated to constant value without the thermal runaway. This is due to the highest sintered density and the lowest leakage current. By the way, the samples sintered at 875 °C exhibited positive creep leakage current in spite of relatively high sintered density and low leakage current comparable with the samples sintered at 850 °C. It can forecast that this sample will cause the thermal runaway.

Figure 6 compares the E–J characteristics after application of a stress with initial E–J characteristics of the samples in accordance with sintering temperature. The nonlinear E–J characteristics of the samples sintered at 800 and 825 °C changed into almost ohmic characteristics after a stress. On

the contrary, the samples sintered at 850 and 875 °C exhibited a small variation in E–J curves after application of a stress. In particular, the samples sintered at 850 °C exhibited the lowest variation of E–J characteristics, when compared with before and after application of a stress.

Figures 7 and 8 compare E_{1mA} and α after application of a stress with initial values in accordance with sintering temperature. The stability can be absolutely estimated through the variations of E_{1mA} and α before and after application of a stress. The samples sintered at 800 and 825 °C exhibited a large variation of E_{1mA} , with $\Delta E_{1mA}/E_{1mA} = -97\%$, after application of a stress. In contrast, the sample sintered at

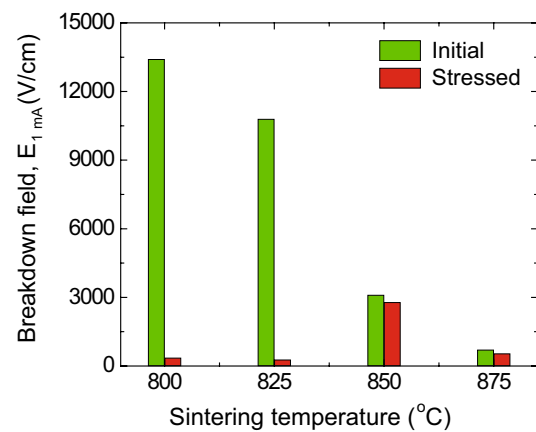
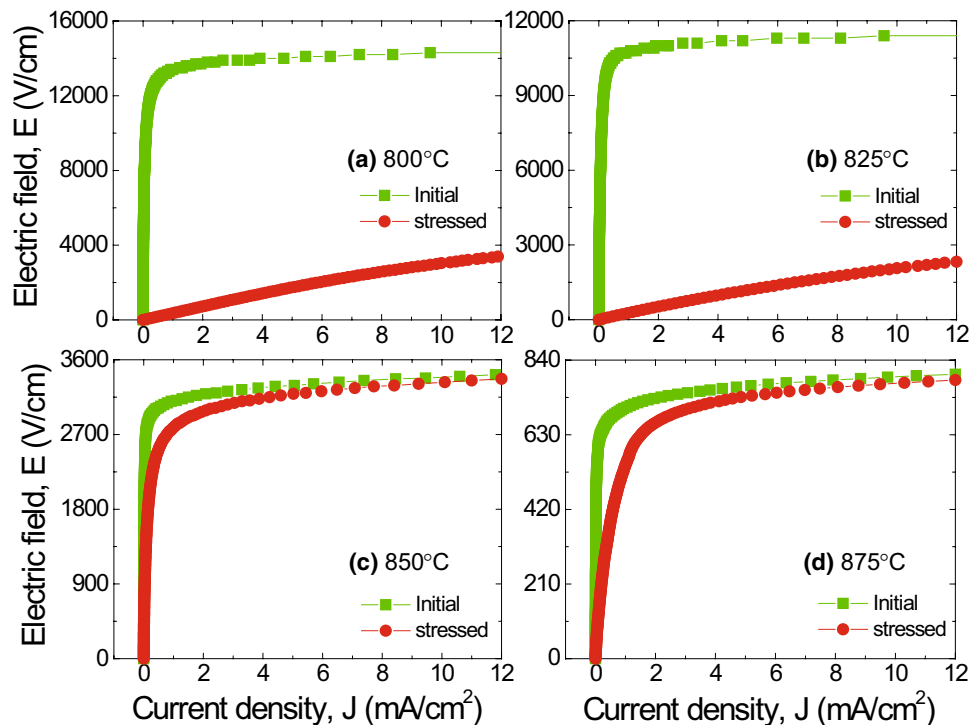


Fig. 7 Behavior of breakdown field of the samples before and after application of a stress as a function of sintering temperature

Fig. 6 E–J characteristic behavior before and after application of a stress of the samples sintered at various temperatures



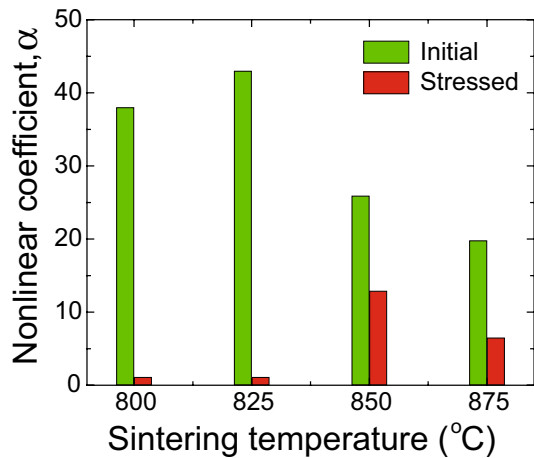


Fig. 8 Behavior of nonlinear coefficient of the samples before and after application of a stress as a function of sintering temperature

Table 2 Variation of breakdown field (E_{1mA}) and nonlinear coefficient (α) before and after application of a stress of the samples sintered at various temperatures

Sintering temp. (°C)	Stress state	E_{1mA} (V/cm)	$\Delta E_{1mA}/E_{1mA}$	α	$\Delta\alpha/\alpha$
800	Initial	13,412	–	38.0	–
	Stressed	358	–97.3	1.1	–97.1
825	Initial	10,797	–	43.0	–
	Stressed	274	–97.5	1.1	–97.4
850	Initial	3104	–	25.9	–
	Stressed	2785	–10.3	12.9	–50.2
875	Initial	706	–	19.8	–
	Stressed	544	–22.9	6.5	–67.2

850 °C exhibited a low variation rate of E_{1mA} , with $\Delta E_{1mA}/E_{1mA} = -10.3\%$, after application of a stress. After application of a stress, the decreasing rate of α value exhibited nearly similar tendency to that of E_{1mA} . These samples sintered at 800 and 825 °C exhibited almost ohmic behavior with $\alpha = 1.1$, after application of a stress. In contrast, the sample sintered at 850 °C exhibited a variation rate of α , with $\Delta\alpha/\alpha = -50.2\%$, after application of a stress. However, a variation rate of α is never small.

In light of above-mentioned discussion, the sample sintered at 850 °C was found to exhibit the strongest stability against a DC stress of ZVMB varistor ceramics. The detailed E–J characteristic parameters before and after application of a stress to the samples sintered at various temperatures are summarized in Table 2.

4 Conclusions

The effect of sintering temperature on microstructure, electrical properties, dielectric characteristics, and DC-accelerated aging behavior of ZVMB ($ZnO-V_2O_5-Mn_3O_4-Bi_2O_3$) varistor ceramics was investigated at the range of 800–875 °C. The average grain size increased the increase of sintering temperature and the sintered density exhibited the highest value at 850 °C. The breakdown field decreased due to the increase in the average grain size with the increase of sintering temperature. The nonlinear coefficient exhibited a maximum value (43.0) at 825 °C and a minimum value (19.8) at 875 °C. The ceramics sintered at 850 °C exhibited the strongest stability under DC-accelerated aging stress of $0.85 E_{1mA}/85^\circ C/24$ h. As a result, the highest nonlinear properties and the strongest stability in ZVMB varistor ceramics were obtained at different sintering temperatures, respectively. The ceramics sintered at 850 °C have a high stability and good nonlinear properties. Therefore, it is necessary to study new additives that can noticeably improve the stability, when sintered at the vicinity of 850 °C in order to apply ZVMB ceramics to multilayered varistors with Ag as an inner electrode.

References

1. M. Matsuoka Jpn. J. Appl. Phys. **10**, 736 (1971)
2. L.M. Levinson, H.R. Philipp, Am. Ceram. Soc. Bull. **65**, 639 (1986)
3. H.R. Pilipp, L.M. Levinson, J. Appl. Phys. **46**, 1332 (1976)
4. T.K. Gupta, J. Am. Ceram. Soc. **73**, 1817 (1990)
5. K. Mukae, K. Tsuda, S. Shiga, IEEE Trans. Power Deliv. **3**, 591 (1988)
6. K. Mukae, Am. Ceram. Bull. **66**, 1329 (1987)
7. A.B. Alles, V.L. Burdick, J. Appl. Phys. **70**, 6883 (1991)
8. A.B. Alles, R. Puskas, G. Callahan, V.L. Burdick, J. Am. Ceram. Soc. **76**, 2098 (1993)
9. Y.S. Lee, K.S. Liao, T.Y. Tseng, J. Am. Ceram. Soc. **79**, 2379 (1996)
10. C.W. Nahm, Mater. Lett. **47**, 182 (2001)
11. J.-K. Tsai, T.-B. Wu, J. Appl. Phys. **76**, 4817 (1994)
12. J.-K. Tsai, T.-B. Wu, Mater. Lett. **26**, 199 (1996)
13. C.-W. Nahm, J. Mater. Sci. **42**, 8370 (2007)
14. C.-W. Nahm, Ceram. Int. **36**, 1109 (2010)
15. C.-W. Nahm, J. Mater. Sci. Mater. Electron. **21**, 540 (2010)
16. C.-W. Nahm, J. Am. Ceram. Soc. **94**, 3227 (2011)
17. C.-W. Nahm, J. Mater. Sci. Mater. Electron. **27**, 9520 (2016)
18. C.-W. Nahm, Ceram. Int. **35**, 541 (2009)
19. C.-W. Nahm, Ceram. Int. **38**, 5281 (2012)
20. C.-W. Nahm, J. Mater. Sci. Mater. Electron. **24**, 4129 (2013)
21. C.-W. Nahm, J. Rare Earth **32**, 29 (2014)
22. C.-W. Nahm, J. Mater. Sci. Mater. Electron. **26**, 168 (2015)
23. C.-W. Nahm, J. Mater. Sci. Mater. Electron. **28**, 903 (2017)
24. J.C. Wurst, J.A. Nelson, J. Am. Ceram. Soc. **55**, 109 (1972)